Supplemental Materials

Molecular Biology of the Cell

Kojer et al.

SUPPLEMENTARY INFORMATION

Kinetic control by limiting glutaredoxin amounts enables thiol oxidation in the reducing mitochondrial IMS

Kerstin Kojer[1], Valentina Peleh[2], Gaetano Calabrese[1], Johannes M Herrmann[2] and Jan Riemer[1]*

[1] Cellular Biochemistry, University of Kaiserslautern, Erwin-Schrödinger-Str. 13, 67663 Kaiserslautern, Germany

[2] Cell Biology, University of Kaiserslautern, Erwin-Schrödinger-Str. 13, 67663 Kaiserslautern, Germany

* address correspondence to J.R.: jan.riemer@biologie.uni-kl.de; tel: +49-6312052885; Cellular Biochemistry, University of Kaiserslautern, Erwin-Schrödinger-Str. 13, 67663 Kaiserslautern, Germany

3 supplementary tables

8 supplementary figures

Supplementary Tables

Table S1. E_{GSH} values, and calculated and experimental redox states of selected IMS proteins.

Protein	E°' [mV][a),c)]	calculated % of oxidation upon full equilibration with the surrounding glutathione pool[a)]		experimental *in vivo* redox state
		cytosol E_{GSH} = -306 mV[b)]	IMS E_{GSH} = -301 mV[b)]	
Tim9 (twin CX_3C)	-310	58	67	n.d.
Tim10 (twin CX_3C)	-320	75	81	93±5% ox.[d)]
Tim13 (twin CX_3C)	-310	58	67	n.d.
Cox17 (twin CX_9C)	-340	93	95	n.d.
Mia40 (CPC-motif)	-290	23	30	74±4% ox.[b)]
Atp23 (structural cysteines)	n.d.	-	-	4 – 5 disulfide bonds (5 = fully oxidized)[e)]
Cmc1 (twin CX_9C)	n.d.	-	-	fully oxidized[f)]
Coa4 (twin CX_9C)	n.d.	-	-	fully oxidized[f)]

a) at pH 7 and 30 °C
b) (Kojer *et al.*, 2012)
c) (Tienson *et al.*, 2009)
d) (Brandes *et al.*, 2011)
e) (Weckbecker *et al.*, 2012)
f) (Bode *et al.*, 2013)

Table S2. Plasmids and yeast strains used in this study

Plasmid	Characteristics	Primer 5'-3'	Restriction
p415[a)]	TEF promoter, *CEN*-plasmid, *LEU2* marker		
p416[a)]	TEF promoter, *CEN*-plasmid, *URA3* marker		
p415-**roGFP2**[b)]	Cytosolic form of roGFP2	*F:* GGATCCATGGAATTCGTGAGCAAGGGC *R:* AAGCTTTTACTTGTACAGCTCGTCCATG	BamHI HindIII
p415-**b_2**	Presequence (1-86) of cytochrome b_2	*F:* TCTAGAATGCTAAAATACAAACCTTTAC TAAAAATC *R:* GGATCCCATATCCAGTTTCGGCTCG	XbaI BamHI
p415-b_2-**roGFP2**[b)]	roGFP2 fused to presequence (1-86) of cytochrome b_2	*F:* GGATCCGAATTCGTGAGCAAGGGCG *R:* AAGCTTTTACTTGTACAGCTCGTCCATG	BamHI HindIII
p415-**Su9**	Presequence (1-69) of subunit 9 of *Neurospora crassa* ATPase	*F:* TCTAGAATGGCCTCCACTCGTG *R:* GGATCCGGAAGAGTAGGCGCGC	XbaI BamHI
p415-Su9-**roGFP2**[b)]	roGFP2 fused to presequence (1-69) of subunit 9 of *Neurospora crassa* ATPase	*F:* GGATCCGAATTCGTGAGCAAGGGCG *R:* AAGCTTTTACTTGTACAGCTCGTCCATG	BamHI HindIII
p416-Grx1-roGFP2[c)]	Cytosolic form of Grx1-roGFP2		
p416-b_2-Grx1-roGFP2 [c)]	IMS form of Grx1-roGFP2		
p416-Su9-Grx1-roGFP2 [c)]	Matrix form of Grx1-roGFP2		
pRS314	*CEN*-plasmid, *TRP1* marker		
pRS314-**EP**	Endogenous promoter of Grx2	*F:* GAGCTCGGGTCATTGCCGTGG *R:* GGATCCGAAACAATATATAACAGTAGT TGG	SacI BamHI
pRS314-EP_**Term**	Endogenous terminator of Grx2	*F:* GAATTCTTTAAATTACGCTAATATCCCC TTCATAATATTTAC *R:* CTCGAGGTGCTAAGTGTGATGAATGC	EcoRI XhoI
pRS314-EP_**cyto-Grx2**_Term	Δ1-34, cytosolic form of Grx2[d)]	*F:* GGATCCATGGTATCCCAGGAAACAGTT *R:* GAATTCCTATTGAAATACCGGCTTCAATA TTTCAGC	BamHI EcoRI
pRS314-EP_**mito-Grx2**_Term	M35V, mitochondrial form of Grx2[d)]	*F:* GGATCCATGGAGACCAATTTTTCCTTCG *R:* GAATTCCTATTGAAATACCGGCTTCAATA TTTCAGC	BamHI EcoRI
pRS314-EP_**b2-Grx2**_Term	Cyto-Grx2 fused to presequence (1-86) of cytochrome b_2	*F:* GGATCCATGCTAAAATACAAACCTTTAC *R:* GAATTCCTATTGAAATACCGGCTTCAATA TTTCAGC	BamHI EcoRI
pRS314-EP_b2-**C27,30S**_Term	Cystein mutation in cyto-Grx2 fused to presequence (1-86) of cytochrome b_2	*F:* GCAGCAAAGACATAC**TCC**CCTTAC**TCT** AAAGCTACTTTGTCTAC *R:* GTAGACAAAGTAGCTTT**AGA**GTAAGG**GG A**GTATGTCTTTGCTGC	Site-directed mutagenesis
pYX142	TPI promoter, *CEN*-plasmid, *LEU2* marker		
pYX142-Atp23-HA[e)]	C-terminal HA-tag on Atp23		
pRSETA-cyto-Grx2	Δ1-34, cytosolic form of Grx2 for expression in *E. coli*	*F:* GGATCCATGGTATCCCAGGAAACAGTT *R:* GAATTCCTATTGAAATACCGGCTTCAATA TTTCAGC	BamHI EcoRI
pGEX-6P-1-Mia40-ΔTM[f)]	Mia40 (284-403) for expression in *E. coli*		

a) (Mumberg *et al.*, 1995)
b) roGFP2 sensors were also used in a p416-vector
c) (Morgan *et al.*, 2011; Kojer *et al.*, 2012)
d) Template for plasmids were kindly provided by J.A.Bárcena, University of Córdoba, Spain
e) (Weckbecker *et al.*, 2012)
f) (Bien *et al.*, 2010)

Table S3. Yeast strains used in this study

Strain	Genotype	Characteristics	Reference
YPH499[a),b),c),d)]	*MATa ura3-52 lys2-801_amber ade2-101_ochre trp1-Δ63 his3-Δ200 leu2-Δ1*		
Δ*grx1*[a)]	YPH499	*GRX1::URA3*	(Eckers *et al.*, 2009)
Δ*grx2* [a)]	YPH499	*GRX2::kan*MX4	(Eckers *et al.*, 2009)
ΔΔ*grx1,2* [a)]	YPH499	*GRX1::URA3*, *GRX2::kan*MX4	(Eckers *et al.*, 2009)
ΔΔΔ*grx1,2,8* [a),c),d),e)]	YPH499	*GRX1::URA3*, *GRX2::kan*MX4, *GRX8::HIS3*	(Eckers *et al.*, 2009)
W303	*MATα ade2-1 ura3-1 his3-11,15 trp1-1 leu2-3,112 can1-100*		
W303A GalL-Erv1	*MATa ade2-1 ura3-1 his3-11,15 trp1-1 leu2-3, 112 can1-100*	*GALL* promoter inserted upstream of *ERV1*	(Bien *et al.*, 2010)
W303A GalL-Erv1 Δ*grx2* [e)]	*MATa ade2-1 ura3-1 his3-11,15 trp1-1 leu2-3, 112 can1-100*	*GRX2*::*kanMX4*	this study
Δ*glr1*[a)]	*MAT*a *his3Δ1 leu2Δ0 met15Δ0 ura3Δ0*	*glr1*::*kan*MX4	(Outten and Culotta, 2004)
Δ*glr1* + cyto-*GLR1* [a)]	*MAT*a *his3Δ1 leu2Δ0 met15Δ0 ura3Δ0*	Cytosolic *GLR1 encoded* on a plasmid containing *LEU2* introduced into Δ*glr1*	(Outten and Culotta, 2004)

a) roGFP2 sensors were introduced into these yeast strains.
b) Grx1-roGFP2 sensors were introduced into this yeast strain.
c) Either the empty pRS314 plasmid, the b_2-Grx2 or the b_2-Grx2(C27S,C30S) plasmid were introduced into these yeast strains.
d) Atp23-HA plasmid was introduced into these yeast strains.
e) Either the cyto-Grx2 or the mito-Grx2 plasmids were introduced into these yeast strains.

Supplementary Figures

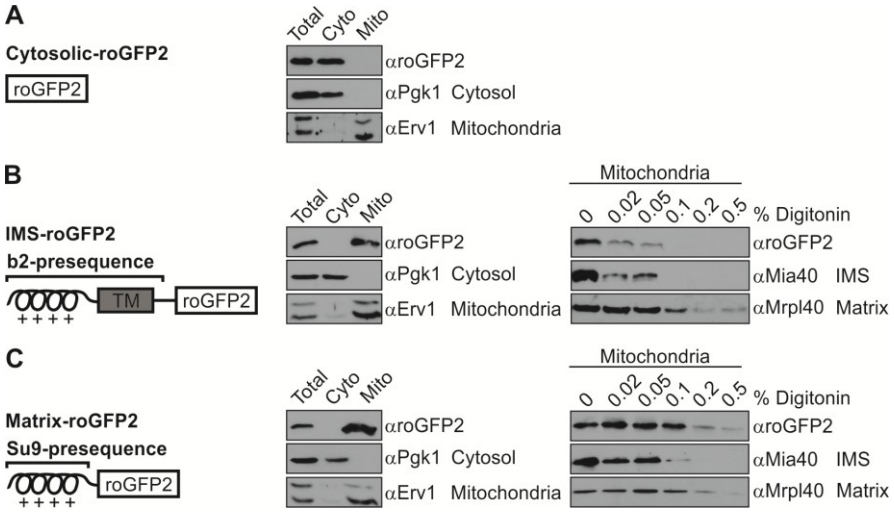

Figure S1. Confirmation of subcellular localizations of roGFP2 sensors.
(A-C) Localizations of roGFP2 probes in yeast cells. The white box represents the roGFP2 protein, the helix represents the amphipathic helix required for matrix targeting, and the grey box represents the hydrophobic sorting domain required for IMS targeting. The targeting sequences of the mitochondrial proteins subunit 9 of the ATPase (Su9, aa 1–69) and cytochrome b_2 (aa 1–86) were fused to roGFP2 (b_2- roGFP2 and Su9- roGFP2). The subcellular localizations of roGFP2 (A), b_2- roGFP2 (Bb) and Su9- roGFP2 (C) were assessed in wild type yeast cells. To this end, cells were grown to mid-log phase in SLac + 0.1% galactose media, they were lysed and fractionated, and fractions were analyzed by SDS–PAGE and immunoblotting using antibodies directed against roGFP2, 3-phosphoglycerate kinase (Pgk1; cytosol), the mitochondrial ribosomal protein Mrpl40 (matrix), Mia40 and Erv1 (both IMS). Cells were fractionated into post-mitochondrial supernatant (Cyto) and mitochondria (Mito). Mitochondria were further subfractionated by treatment with different amounts of digitonin and centrifugation. Pellet fractions were treated with proteinase K. Su9- roGFP2 and b_2- roGFP2 behave like Mrpl40 and Mia40, respectively. Thus, all three sensors localize exclusively to the expected compartments.

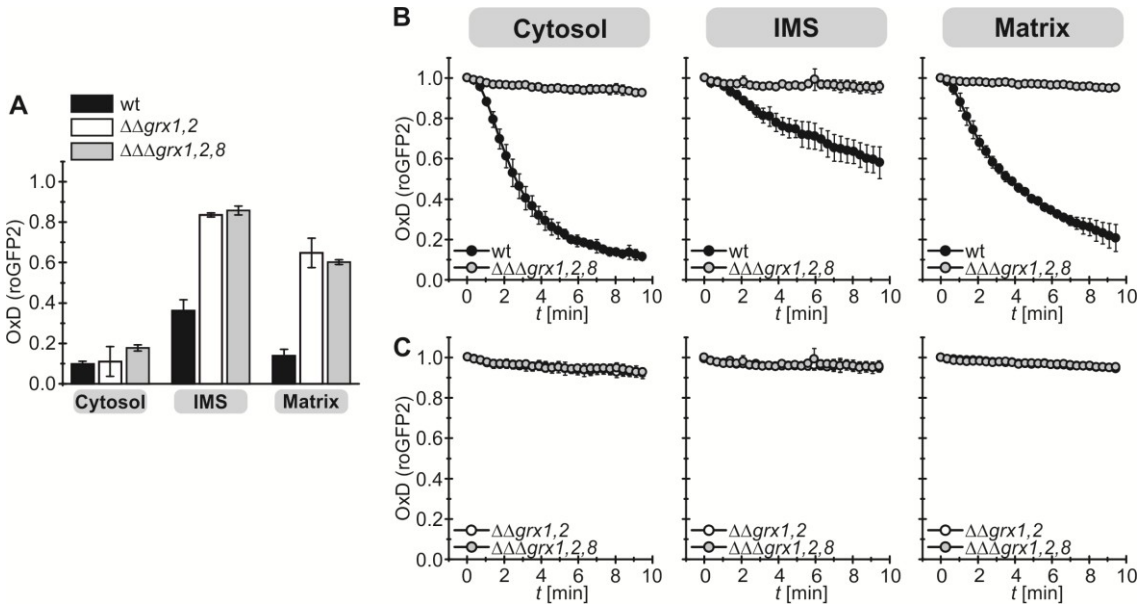

Figure S2. Deletion of *GRX8* in addition to *GRX1* and *GRX2* does not alter the redox state and the dynamic behavior of the roGFP2 probe.

(A) Steady states of the cytosolic and mitochondrial roGFP2 sensors (roGFP2, Su9- roGFP2, b_2- roGFP2) in yeast deletion mutants of *GRX1* and *GRX2* or *GRX1*, *GRX2* and *GRX8*, respectively. Experiments were performed as described in Figure 1. **(B)** Recovery kinetics after diamide shock performed on *ΔΔgrx1,grx2* and *ΔΔΔgrx1,grx2,grx8* cells. Cells expressing roGFP2, Su9-roGFP2 and b_2-roGFP2 were analyzed as described in Figure 1. Reported values are the mean of three independent experiments. Error bars are the means ± s.d.

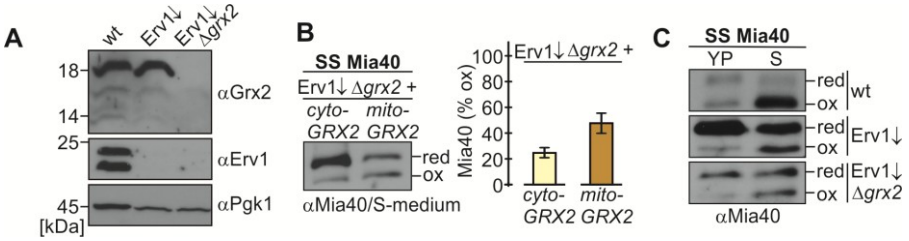

Figure S3. The cytosolic form of Grx2 couples Mia40 to the IMS glutathione pool.

(A) Strains for Mia40 redox state determination. We designed strains that contained Erv1 under the control of a regulatable promoter and in addition either expressed or lacked Grx2. Cells were grown to mid-log phase in glucose media to lower Erv1 levels. Then, they were lysed and analyzed by SDS–PAGE and immunoblotting using antibodies directed against Grx2, Erv1 and Pgk1 as loading control. **(B)** Dependence of Mia40 redox state on different variants of Grx2 (cyto- and mito-Grx2). Cells lacking *GRX2* and depleted of Erv1 were transformed with plasmids expressing either cyto- or mito-Grx2. Cells were grown in S-medium containing glucose to mid-log phase and the redox state of Mia40 was determined as described in Figure 3. SS; steady state. Reported values are the mean of three independent experiments. Error bars are the means ± s.d. **(C)** Dependence of the Mia40 redox state on the growth medium. Different cells were grown in S- or YP-medium and the Mia40 redox state at steady state (SS) was analyzed as described in Figure 3. The redox state of Mia40 is in general more oxidized in S-medium. Please note that the Mia40 redox states in Figure 3 were determined after growth in YP-medium, while the ones in Figure 4 after growth in S medium.

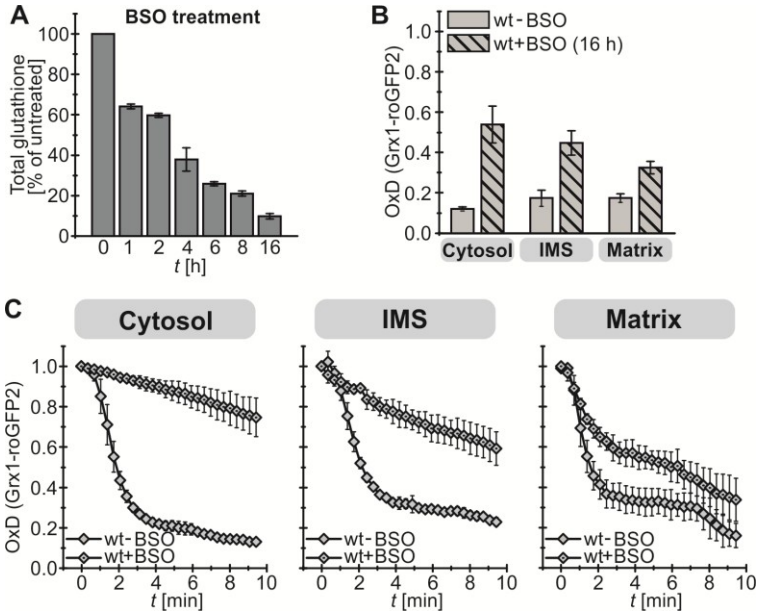

Figure S4. Treatment of cells with buthionine sulfoximine (BSO) results in glutathione depletion, a more oxidized E_{GSH} and a slower recovery of Grx1-roGFP2 after oxidative stress.

(A) Glutathione amounts in whole cells during BSO treatment. After different times in the presence of BSO cells were collected by sulfosalicylic acid precipitation and glutathione levels were measured using a 5,5'-dithiobis-(2-nitrobenzoic acid) (DTNB) cycling assay (Minich *et al.*, 2006). **(B)** Steady states of the cytosolic and mitochondrial Grx1-roGFP2 sensors in yeast cells treated with BSO for 16 h. Experiments were performed as described in Figure 1. BSO treatment increases the OxD in all compartments (*i.e.* probes and consequently E_{GSH} become more oxidized). **(C)** Recovery kinetics after diamide shock on cells treated with BSO for 16 h. Cells expressing Grx1-roGFP2 sensors targeted to the indicated compartments were analyzed as described in Figure 1. BSO treatment delays recovery of sensors in all compartments, most strongly in the cytosol and the IMS. Reported values are the mean of three independent experiments. Error bars are the means ± s.d.

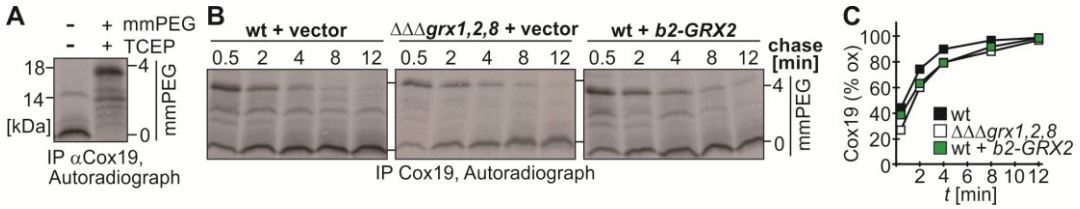

Figure S5. Cox19 is oxidized with a half time of less than two minutes, and its oxidation is not affected by expression of b_2-Grx2

(A) mmPEG24 alkylation of Cox19. Cells were radioactively labeled, precipitated with TCA, and samples were treated with buffer or TCEP and mmPEG24. Samples were analyzed by SDS-PAGE and autoradiography. The reduced and oxidized states of Cox19 can be distinguished. **(B)** *In-vivo* oxidation kinetics of Cox19 in wild type cells expressing or not expressing b_2-Grx2, and in *GRX1, GRX2, GRX8* deletion cells. Experiments were performed as described in Figure 5B. Cox19 oxidation is not affected by the presence or absence of Grx2 in the IMS. **(C)** Quantification of the results obtained in (B).

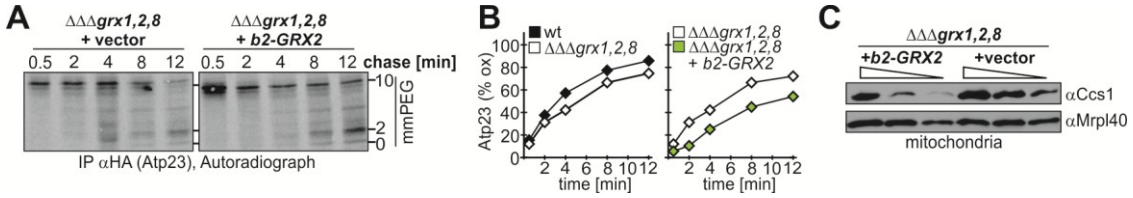

Figure S6. Atp23-HA oxidation is delayed upon overexpression of b_2-Grx2 in *GRX1, GRX2, GRX8* triple deletion cells.

(A) *In-vivo* oxidation kinetics of Atp23-HA in *GRX1, GRX2, GRX8* deletion cells expressing or not expressing b_2-Grx2. Experiments were performed as described in Figure 5B. Atp23-HA oxidation is delayed by the presence of additional Grx2 in the IMS. **(B)** Quantification of the results obtained in (a) and Figure 5d. Notably, *GRX1, GRX2, GRX8* deletion slightly delays oxidative folding of Atp23-HA in comparison to the wild type. **(C)** Ccs1 does accumulate to a lower extent in the presence of b_2-Grx2 also in a *GRX1, GRX2, GRX8* deletion background. The experiment was performed as described in Figure 5F

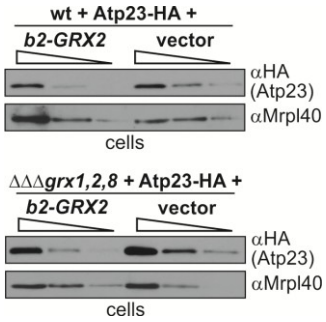

Figure S7. Atp23-HA levels are slightly decreased in cells coexpressing b_2-Grx2.

Cells from the indicated strains were analyzed by SDS-PAGE and immunoblotting against HA and Mrpl40. Steady state levels of Atp23-HA are mildly affected by differences in Grx levels in the IMS.

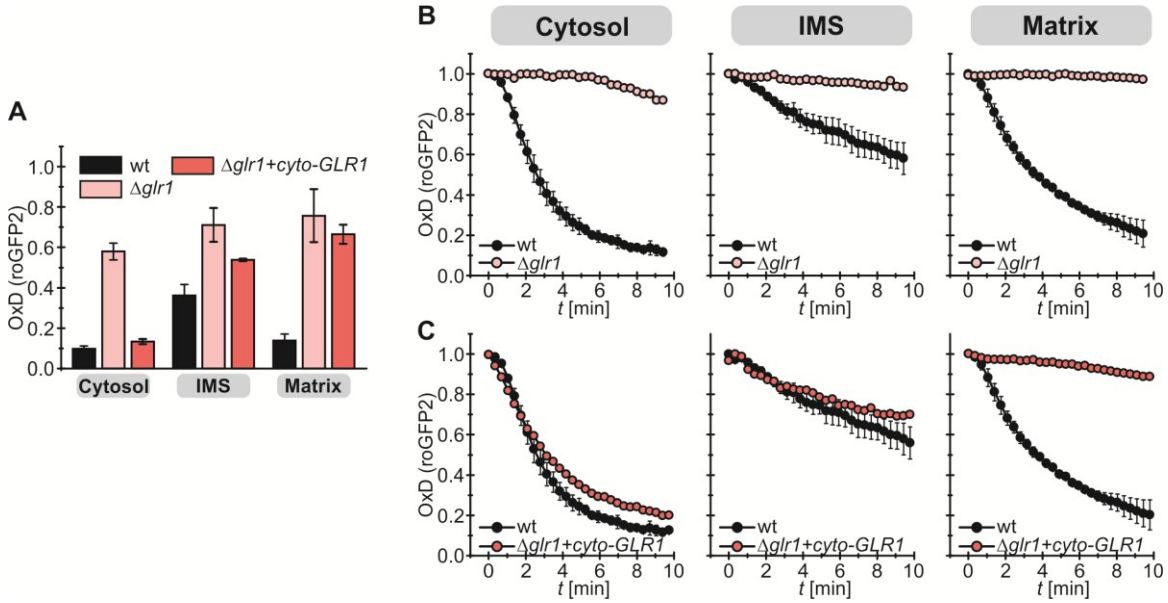

Figure S8. Like the Grx1-roGFP2 probe the roGFP2 probe reports a dependence of the IMS glutathione pool on cytosolic glutathione reductase (Glr1).

(A) Steady states of the cytosolic and mitochondrial roGFP2 sensors in yeast cells lacking *GLR1* or expressing the cytosolic form of the protein. Experiments were performed as described in Figure 1. Deletion of *GLR1* leads to more oxidized roGFP2 redox states in all compartments. Expression of the cytosolic form of Glr1 in this background complements the phenotype in the cytosol but not in the matrix and only in part in the IMS. **(B, C)** Recovery kinetics after diamide shock on cells lacking *GLR1* or expressing the cytosolic form of the protein. Cells expressing roGFP2 sensors targeted to the indicated compartments were analyzed as described in Figure 1. Deletion of *GLR1* abolishes recovery of roGFP2 in all compartments. In line with the steady state findings expression of cytosolic Glr1 results in recovery in the cytosol but not in the matrix. In the IMS the roGFP2 probe also recovers albeit apparently to a higher OxD than in the wild type. This indicates that cytosolic Glr1 enables a reducing glutathione pool also in the IMS. Reported values are the mean of two to three independent experiments. Error bars are the means ± s.d.

Supplementary Methods

Growth of yeast cells - Cells were grown in YP-media. For all experiments using plasmid-containing strains cells were grown in synthetic medium (0.17 % yeast nitrogen base, 0.5 % $(NH_4)_2SO_4$, pH 5.5) containing drop-out-mix lacking uracil, leucine and tryptophane respectively (20 mg/l adenine sulfate, 20 mg/l, L-arginine, 20 mg/l L-histidine, 30 mg/l L-isoleucine, 30 mg/l L-lysine, 20 mg/l L-methionine, 50 mg/l L-phenylalanine, 20 mg/l L-threonine, 20 mg/l L-tyrosine, 150 mg/l L-valine) supplemented with 2 % galactose or 2 % glucose, respectively.

Submitochondrial fractionation – Subcompartments of mitochondria were analysed by incubation with increasing concentrations of digitonin on ice for 3 min. Subsequently, proteinase K (0.1 mg/ml final concentration, 20 min on ice) was added to remove released proteins. The reaction was stopped by addition of PMSF (2 mM final concentration), and after centrifugation pellets were resuspended in sample buffer (60 mM Tris HCl pH 6.8, 2 % (w/v) SDS, 10 % glycerol, 0.05 % (w/v) bromphenol blue) and samples were analyzed by reducing SDS-PAGE and Western Blot.

Determination of cellular glutathione amounts –This assay was essentially performed as described previously (Minich *et al.*, 2006).

Buthionine sulfoximine (BSO) treatment – Yeast strains were grown in galactose-containing media to mid-log phase and treated with 1 mM BSO for up to 16 h.

OxD and E_{GSH} calculations – The following equation was used to calculate the degree of oxidation (OxD) of the probe:

$$OxD = \frac{R - R(red)}{I_{488}(ox) \Big/ I_{488}(red) * (R(ox) - R) + (R - R(red))}$$

I_n = intensity at a given wavelength n; I_{488}(ox), I_{488}(red) = intensities at 488 nm upon complete oxidation or reduction, respectively; R = I_{405}/I_{488}; R(ox) = I_{405}/I_{488} upon complete oxidation; R(red) = I_{405}/I_{488} upon complete reduction

Upon full equilibration of the sensor with the surrounding glutathione pool E_{GSH} can be calculated as follows:

$$E_{GSH} = E_{roGFP2} = E^{\circ'}_{roGFP2} - \frac{RT}{2F} \ln \left(\frac{1 - OxD}{OxD}\right)$$

R is the gas constant (8.315 J $K^{-1}mol^{-1}$), T the absolute temperature (303.15 K), F the Faraday constant (96,485 C mol^{-1}) and $E^{\circ'}_{roGFP2}$ = -280 mV (Dooley *et al.*, 2004)

The predicted values of oxidation upon full equilibration with the surrounding glutathione pool results from the OxD calculated by the following equation:

$$OxD = \left(\frac{1}{e^x + 1}\right)$$

$$x = \frac{2F(-E_{GSH} + E^{\circ'})}{RT}$$

References for supplementary information

Bien, M., Longen, S., Wagener, N., Chwalla, I., Herrmann, J.M., and Riemer, J. (2010). Mitochondrial disulfide bond formation is driven by intersubunit electron transfer in Erv1 and proofread by glutathione. Mol Cell *37*, 516-528.

Bode, M., Longen, S., Morgan, B., Peleh, V., Dick, T.P., Bihlmaier, K., and Herrmann, J.M. (2013). Inaccurately assembled cytochrome c oxidase can lead to oxidative stress-induced growth arrest. Antioxid Redox Signal *18*, 1597-1612.

Brandes, N., Reichmann, D., Tienson, H., Leichert, L.I., and Jakob, U. (2011). Using quantitative redox proteomics to dissect the yeast redoxome. J Biol Chem *286*, 41893-41903.

Dooley, C.T., Dore, T.M., Hanson, G.T., Jackson, W.C., Remington, S.J., and Tsien, R.Y. (2004). Imaging dynamic redox changes in mammalian cells with green fluorescent protein indicators. J Biol Chem *279*, 22284-22293.

Eckers, E., Bien, M., Stroobant, V., Herrmann, J.M., and Deponte, M. (2009). Biochemical characterization of dithiol glutaredoxin 8 from Saccharomyces cerevisiae: the catalytic redox mechanism redux. Biochemistry *48*, 1410-1423.

Kojer, K., Bien, M., Gangel, H., Morgan, B., Dick, T.P., and Riemer, J. (2012). Glutathione redox potential in the mitochondrial intermembrane space is linked to the cytosol and impacts the Mia40 redox state. EMBO J *31*, 3169-3182.

Minich, T., Riemer, J., Schulz, J.B., Wielinga, P., Wijnholds, J., and Dringen, R. (2006). The multidrug resistance protein 1 (Mrp1), but not Mrp5, mediates export of glutathione and glutathione disulfide from brain astrocytes. J Neurochem *97*, 373-384.

Morgan, B., Sobotta, M.C., and Dick, T.P. (2011). Measuring E(GSH) and H(2)O(2) with roGFP2-based redox probes. Free Radic Biol Med *51*, 1943-1951.

Mumberg, D., Muller, R., and Funk, M. (1995). Yeast vectors for the controlled expression of heterologous proteins in different genetic backgrounds. Gene *156*, 119-122.

Outten, C.E., and Culotta, V.C. (2004). Alternative start sites in the Saccharomyces cerevisiae GLR1 gene are responsible for mitochondrial and cytosolic isoforms of glutathione reductase. J Biol Chem *279*, 7785-7791.

Tienson, H.L., Dabir, D.V., Neal, S.E., Loo, R., Hasson, S.A., Boontheung, P., Kim, S.K., Loo, J.A., and Koehler, C.M. (2009). Reconstitution of the mia40-erv1 oxidative folding pathway for the small tim proteins. Mol Biol Cell *20*, 3481-3490.

Weckbecker, D., Longen, S., Riemer, J., and Herrmann, J.M. (2012). Atp23 biogenesis reveals a chaperone-like folding activity of Mia40 in the IMS of mitochondria. EMBO J *31*, 4348-4358.